Energy Based Cutting Force Model Calibration for Milling

Min Xu[1], Robert B. Jerard[2] and Barry K. Fussell[3]

[1]University of New Hampshire, mxu@unh.edu
[2]University of New Hampshire, robert.jerard@unh.edu
[3]University of New Hampshire, barry.fussell@unh.edu

ABSTRACT

Accurate estimation of cutting forces requires that the predictive model be properly calibrated. Calibration typically requires a time consuming process and an expensive force measurement device. In this paper, an energy based process is described for calibrating a force estimation model using motor spindle power. Experimental results for flat and ball end mills are given. The method has been shown to be accurate for estimating forces for a wide variety of cutting conditions. Furthermore, we show how the calibration process can be done either off-line with a quick and simple process, or on-line while cutting in a production process. An additional benefit of the method is that the continuous calibration process can be used to help diagnose tool wear.

Keywords: Models, calibration, spindle power, energy based.

1. INTRODUCTION

Cutting force models can play an important role in setting cutting conditions that are safe, efficient and produce parts of the desired quality. Unfortunately, the models are only as accurate as the model coefficients which are a function of the cutting tool and the workpiece material. The coefficients are also a function of tool wear, which typically results in increased cutting forces as the tool wears.

There has been significant research reported in modeling the mechanics of milling. A series of papers by Kline et al. [7, 14] presented a mechanistic model which considers the tangential cutting force to be proportional to the chip load and the radial force to be proportional to the tangential force. The size effect is captured by the nonlinear empirical relationship between specific energy and uncut chip thickness. Altintas presented a linear edge effect model in which the tangential force is split into a cutting component and a parasitic component (also known as an edge, rubbing or plowing force) [1]. In this model, cutting forces are linearly proportional to both chip thickness and contact area. Both models have been shown to be reasonably accurate at force prediction when model coefficients are properly calibrated [8-13].

A number of different methods have been used for model calibration. Budak et al. presented a unified mechanics of cutting approach in predicting the milling force coefficients for cylindrical helical end mills [4]. It is shown that the milling force coefficients for all force components and cutter geometries can be predicted from an orthogonal cutting database and the generic oblique cutting analysis for use in the predictive mechanistic milling models. Lee et al. further extended the approach to helical ball end mills [15]. The cutting force distribution on the helical ball-end mill flutes is accurately predicted by the proposed method. However, some cutting tools may have complex cutting edges, and the evaluation of cutting constants by orthogonal cutting tests may be time-consuming.

The model coefficients can also be identified through empirical curve fit either to measured average milling forces or to instantaneous forces [14]. The least square fit method is widely used in force model calibration by trying to either fit the force profile of one specific cut [3, 23] or average force for a number of cuts [1, 16]. By investigating milling forces in the frequency domain, Zhang et al. provided an improved method to calibrate the cutting coefficients [24]. The validity of the method is confirmed based on a series of experiments and numerical simulations.

All these calibration methods are based on instantaneous or average force measurement. Sensors used to measure cutting forces can be expensive and adversely affect machine stiffness. This prevents the force prediction techniques

from being used in industry. In contrast, a power sensor is inexpensive and non-invasive. Power sensors have been widely used for tool condition monitoring in both academic research [20] and industrial applications [2]. In this paper, a power based calibration method based on the linear edge effect tangential force model is presented with the intention of quick and accurate model calibration as the tool wears.

2. FORCE MODEL

The energy based calibration method assumes that the model is linear with chip thickness and contains edge forces. The tangential force is split into a cutting component and a parasitic component. The instantaneous tangential force at a particular tool rotation angle ϕ is:

$$\Delta F_T(\phi,u) = K_{TC}\, h(\phi,u)\,\Delta u + K_{TE}\,\Delta u \tag{2.1}$$

where Δu is the length along the periphery of the cutter, K_{TC} is the tool/material cutting energy, N/mm^2 in the tangential direction, and K_{TE} is the tool/material edge force, N/mm in the tangential direction. The model assumes a zero helix angle for a tooth for any discrete slice of the tool. The normal force and the longitudinal component (perpendicular to tangential and normal direction) can be similarly expressed.

$$\Delta F_N(\phi,u) = K_{NC}\, h(\phi,u)\,\Delta u + K_{NE}\,\Delta u \tag{2.2}$$

$$\Delta F_A(\phi,u) = K_{AC}\, h(\phi,u)\,\Delta u + K_{AE}\,\Delta u \tag{2.3}$$

where ΔF_T and ΔF_N directions are defined in Fig. 1. and ΔF_A is generally in the negative Z direction.

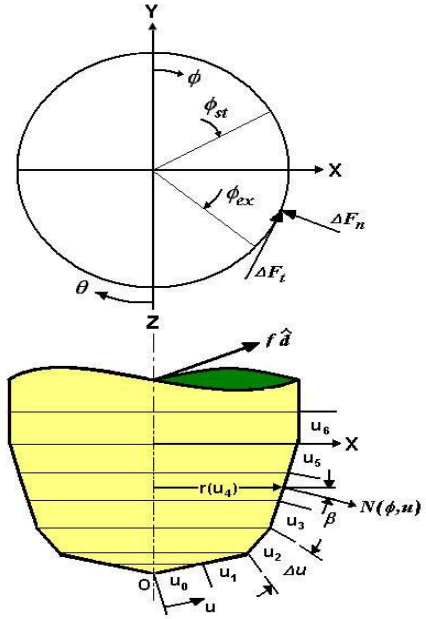

Fig. 1: The cutting tool is discretized into disc elements defined by equal increments along the periphery.

Fig. 1 shows a general cutting tool. The xyz local coordinate system is defined relative to the cutting tool. The milling forces and cut geometry are defined relative to this system, which is local to the cutting tool and varies with the direction of motion, denoted by velocity vector $f\,\hat{d}$ (velocity vector of magnitude f (mm/s) in the direction $\hat{d}$). The local x coordinate axis is normal to the axial direction z, with $f\,\hat{d}$ lying in the local x-z plane. Angle ϕ is the location of the cutting edge measured from the Y axis, for some arbitrary tool rotation angle θ. β is the angle between the surface normal $\mathbf{N}(\phi,u)$ and the horizontal X-Y plane.

The chip thickness $h(\phi,u)$ at any location on the cutter is the scalar product of the velocity vector with the cutter surface normal $\mathbf{N}(\phi,u)$, divided by the number of teeth (n_t) times the spindle speed ω (rev/s) [5].

$$h(\phi,u) = \frac{f\,\hat{d}\cdot\mathbf{N}(\phi,u)}{n_t\,\omega} \tag{2.4}$$

The force on a differential tooth element has tangential, normal and longitudinal components. The tangential force is located in the x-y plane of Fig. 1., while the normal component is in the opposite direction of the surface normal $\mathbf{N}(\phi,u)$.

The total cutting force can be determined for a given tool position angle θ by:

$$\begin{aligned}
F_x(\theta) &= \sum_{i=1}^{n_u}\sum_{j=1}^{n_t}\left\{-\Delta F_T\cos\phi - \Delta F_N\sin\phi\,\cos\beta - \Delta F_A\sin\phi\,\sin\beta\right\}\\
F_y(\theta) &= \sum_{i=1}^{n_u}\sum_{j=1}^{n_t}\left\{\Delta F_T\sin\phi - \Delta F_N\cos\phi\,\cos\beta - \Delta F_A\cos\phi\,\sin\beta\right\}\\
F_z(\theta) &= \sum_{i=1}^{n_u}\sum_{j=1}^{n_t}\left\{\Delta F_N\sin\beta - \Delta F_A\cos\beta\right\}
\end{aligned} \tag{2.5}$$

where ΔF_T, ΔF_N, and ΔF_A, are calculated using Eqn. 2.1.-2.3., n_u is the total number of elements, n_t is the number of teeth, and β is the angle between the surface normal of the element u, and the x-y plane as shown in Fig. 1. The resultant force in the x-y plane F_{xy} is usually of greatest importance as it is used to calculate tool deflections and bending stresses.

$$F_{xy}(\theta) = \sqrt{F_x^2(\theta) + F_y^2(\theta)} \tag{2.6}$$

3. TANGENTIAL CUTTING COEFFICIENTS

The energy required to remove an infinitesimal element of material is:

$$dE = K_{TC}\,h(u,\phi)\,r(u)\,d\phi\,du + K_{TE}\,r(u)\,d\phi\,du \tag{3.1}$$

The cutter consists of one or more teeth, each of which can be divided into one or more segments which have similar values of K_{TC} and K_{TE}. For example, the teeth on the end of a flat end cutter may have different geometry than the teeth on the side and therefore exhibit different cutting coefficients. Different segments of the tool may also exhibit different values of the coefficients due to wear effects.

The total energy required to remove material for the i_{th} segment of the j_{th} tooth during a single revolution of the cutter can be obtained through integration:

$$E_{ij} = K_{TC_{ij}}\int_{u_m}^{u_n}\int_{\phi_{ent}}^{\phi_{ext}} h(u,\phi)\,r(u)\,d\phi\,du + K_{TE_{ij}}\int_{u_m}^{u_n}\int_{\phi_{ent}}^{\phi_{ext}} r(u)\,d\phi\,du \tag{3.2}$$

where u is the distance traced along the profile of the cutter as illustrated in Fig. 1.

Noting that the material removed Q_{ij} is equal to:

$$Q_{ij} = \int_{u_m}^{u_n}\int_{\phi_{ent}}^{\phi_{ext}} h(u,\phi)\,r(u)\,d\phi\,du \tag{3.3}$$

and the area of contact between the cutter and the workpiece is:

$$A_{ij} = \int_{u_m}^{u_n}\int_{\phi_{ent}}^{\phi_{ext}} r(u)\,d\phi\,du \tag{3.4}$$

We can express the energy in terms of material removed and contact area:

$$E_{ij} = \left[K_{TC}Q + K_{TE}A\right]_{ij} \tag{3.5}$$

And the total energy for the entire cutter is:

$$E_{tot} = \sum_j \sum_i E_{ij} \tag{3.6}$$

Because the analysis is based on energy, the helix angle associated with the teeth can be ignored when performing the integrations in Eqn. (3.2) and a straight flute is assumed.

In order to take the coefficients outside of the integral in Eqn. (3.2) it is assumed that they are not a function of chip thickness and models which assume a non-linear relationship between chip thickness and force may not be used in this manner [14]. The linear model used in this analysis compares well in force prediction with the more complex models that include chip thickness in the coefficients [13].

The average motor power needed to remove the material from the workpiece is related to the energy:

$$P_{avg} = \frac{E_{tot}}{\tau} = \sum_j \sum_i \frac{E_{ij}}{\tau} = \sum_j \sum_i \left[K_{TC}\ \dot{Q}\ + K_{TE}\ \dot{A}\ \right]_{ij} \tag{3.7}$$

where τ is the tool rotation period in seconds:

$$\tau = \frac{60}{\omega} \tag{3.8}$$

and ω is the spindle speed in revolutions per minute. The volumetric removal rate and cutting area rate are:

$$\dot{Q}_{ij} = \frac{Q_{ij}}{\tau} \qquad \dot{A}_{ij} = \frac{A_{ij}}{\tau} \tag{3.9}$$

The power defined in Eqn. (3.7) can only come from two sources: spindle power and feed drive power. Since the motor spindle power is generally 100-1000 times larger than feed drive power the contribution from the feed drive power can be ignored.

4. MODEL CALIBRATION

A power sensor is used to measure the electrical power P_e to the motor. The available mechanical power P_m can be calculated by multiplying the electrical power times the motor efficiency η_e. During machining, the mechanical power P_m includes two components: 1) P_f, the power to overcome the mechanical friction in the motor and drive system and 2) P_c, the power actually used in cutting the part.

$$P_m = P_e * \eta_e = P_f + P_c \tag{4.1}$$

When the spindle motor runs at a constant speed without cutting any material, the measured electrical power is the tare power P_t. As Pc equals zero, we get:

$$P_t * \eta_e = P_f \tag{4.2}$$

If we assume that the frictional losses are constant for a given spindle speed and that the cutting power is defined by Eqn. (3.7) we get:

$$P_m = P_t * \eta_e + P_c = P_t * \eta_e + K_{TC} * \dot{Q} + K_{TE} * \dot{A} \tag{4.3}$$

where K_{TC} and K_{TE} are assumed uniform over the calibration cut. The effect of coefficient variation is minimized by selecting appropriate cut geometry for calibration; a contact area where the tool geometry is constant, or over a number of contact areas to find average coefficients. Average coefficients result in a robust model that is able to predict cutting power reasonably well for a large variety of contact areas, spindle speeds, and feedrates.

In our previous research [11-13, 22], tare power P_t was measured and then subtracted from measured power P_e to perform model calibration and obtain coefficients K_{TC} and K_{TE} based on Eqn. (4.3). The tare power is a function of spindle speed and motor temperature [6] and it is therefore important that it be measured frequently, at the same spindle speed as used in cutting and not too long before the cutting takes place. This will require time and may not be feasible. Instead $P_t * \eta_e$ can be treated as an unknown. With a minimum of three experiments, the coefficients K_{TC}, K_{TE} and the quantity $P_t * \eta_e$ can be found using Eqn (4.3). In fact, it is usually advantageous to perform many more than the minimum and rely on a least squares fit. In matrix form,

$$[P_m] = \begin{bmatrix} 1 & \dot{Q} & \dot{A} \end{bmatrix} \begin{bmatrix} P_t * \eta_e \\ K_{TC} \\ K_{TE} \end{bmatrix} = [G][K] \tag{4.4}$$

$$\mathrm{K} = \left[G^T\ G\right]^{-1} G^T\ P_m \tag{4.5}$$

Where the G matrix is defined by cutting geometry, and P_m is the measured power for each cut, determined from $P_e * \eta_e$. To be solvable, the G matrix of Eqn. (4.4) must not be singular and should not be ill-conditioned. Proper choice of experiments will prevent this unwanted result.

The motor efficiency value η_e can either be determined by system calibration with a dynamometer or be obtained from the motor manufacturer. Fig. 2 is a typical induction motor efficiency curve. To automate the model calibration process, a look-up table for all motor conditions can be formed based on the curve.

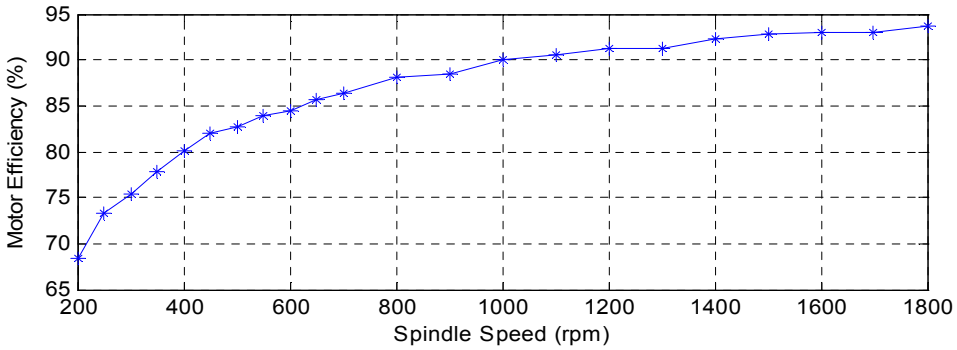

Fig. 2: Motor efficiency curve.

Power sensors typically do not have the frequency bandwidth necessary to measure instantaneous power at the tooth passing frequency. Filters are used to remove high frequency noise, limiting bandwidth, but providing a fairly clean signal for the average power. Results from our setup yield a resolution of 0.02 kw, when averaging 10 spindle revolutions of power data.

The normal and longitudinal coefficients are also needed to estimate force. For a flat end cutter, only tangential and normal coefficients are necessary to estimate F_{xy}. The normal coefficients can vary depending on cutter geometry and workpiece material. Some researchers have assumed a ratio of 0.3 between normal and tangential coefficients [19, 21]. Using force data obtained from calibration cuts (Section 6.1.1), we found $K_{NC} = 0.395\ K_{TC}$, and $K_{NE} = 0.566\ K_{TE}$. In normal machine operation, force data would not be available to find these ratios. A conservative approach would be to use the largest expected ratios, e.g. 0.7, to estimate the resultant force.

5. GEOMETRIC ANALYSIS

An extended Z-buffer method [5] is selected for use in the geometric model of the workpiece. The tool is modeled by slicing into discs perpendicular to the z axis. The tool should not be sliced into equal thickness, but into equal Δu increments along the periphery as shown in Fig. 1. The entrance and exit angles for the teeth can be calculated from the radial depth of each disc [9]. A numerical summation can be used to find Q and A for a tool segment as shown in the pseudo-code in Tab. 1.

Our research group has spent considerable effort on the geometric modeling of 3 and 5 axis machining [5, 9] and is pleased to see that this technology has progressed to the point of commercial application. Therefore, a toolkit from Predator [18] is used to find the entrance and exit angles at each value of u. The Predator toolkit finds the contact between the tool and the workpiece for any given tool move, and keeps a history of the part shape. Tool surfaces perpendicular to the z axis, such as the bottom of a flat end mill, need to be handled a little differently and are treated as a series of annular rings.

Q = 0, A = 0 (initialize Q, A, volume and contact area)
for u = 0 to n_u step Δu
  for ϕ = ϕ_{st} to ϕ_{ex} step Δϕ
    Q = Q + h(u, ϕ) r(u)ΔϕΔu (Accumulate volume removed)
    A = A + r(u) ΔϕΔu (Accumulate surface area swept)
  end ϕ
end u
$\dot{Q} = \frac{Q}{\tau}$ $\dot{A} = \frac{A}{\tau}$ (divide total volume and swept area by time period)

Tab. 1: Procedure for Model Calibration.

6. EXPERIMENTAL RESULTS

6.1 Power Model Verification

A robust machining power estimation model must be able to maintain accuracy for a variety of cutting conditions. The calibrations have been performed on a wide variety of materials using a number of different cutting tools. Power is measured using a universal power sensor from Load Controls Inc. Force is measured with a Kistler 9257B table dynamometer. Power and force data are sampled at 3 degree intervals of tool rotation.

6.1.1 Flat-end Mill Test

A standard calibration test is developed that includes eight different cutting geometries (slot, upmill, downmill and center cut) with four different feeds, for a total of 32 different tests. A two flute, 25.4 mm (1.0 inch) flat end cutter, runout 0.0127 mm, rotating at 1337 rpm, is used to machine 6061-T6 aluminum at an axial depth of 3.81 mm. Tab. 2 and 3 summarize the different conditions for flat end mill cutter. Tab. 2 entries are correlated with Fig. 3., e.g. the first entry is for slot cutting and the first four data points shown in the figure are for slot cutting at the four different feeds shown in Tab. 3. Surface speed and maximum feed per tooth are selected from recommended values from tables [17] to calculate spindle speed and feedrates. Feedrates are chosen to be 50%, 75%, 90% and 110% of recommended value to generate a good distribution of material removal rates. The force model coefficients obtained from the calibration cuts using power measurements and Eqn. (4.5) are: K_{TC} = 693.8 N/mm^2, K_{TE} = 18.98 N/mm. The normal coefficients obtained from the measured forces are K_{NC} = 0.395 K_{TC}, and K_{NE} = 0.566 K_{TE}. Figure 3 shows excellent agreement between measured and estimated power (maximum error = 4%) and very good agreement between measured and estimated maximum results forces (maximum error = 16%). (Refer to [8] for description of calculation of resultant force including tool runout). Fig. 4 shows a typical comparison between the measured and estimated resultant force profile as a function of rotation angle.

test	1 (slot)	2(up)	3 (up)	4 (up)	5 (center)	6 (down)	7 (down)	8 (down)
ϕ st	0 (deg)	60	90	120	75	0	0	0
η ex	180 (deg)	180	180	180	105	120	90	60

Tab. 2: Entrance and exit angles (degrees) for different machining geometries.

	f1	f2	f3	f4
fpt (mm)	0.07112	0.10922	0.13208	0.16002

Tab. 3: Feed per tooth (mm/tooth) for Aluminum 6061.

Circular tool moves at different radii are also performed with a flat end mill cutter to validate the model. The same tangential model coefficients determined from the calibration cuts are used in estimating the power. Specific conditions, measured power and calculated values for $\dot{Q}$ and $\dot{A}$ are listed in Tab. 4. The value of P_m (Tab. 4) equals the electrical power P_e multiplied by the motor efficiency η_e (Figure 2), and the estimated P_m is calculated from the right side of Eqn. (4.3). Fig. 5 shows the good agreement between the power estimation and the measured power. For

upmill and downmill cuts with circular tool moves at same cutting conditions, the average power is not the same as it is for the linear tool move cases (G code = G1). For circular moves (G code = G2/G3) the actual feedrate varies from the inner to the outer side of the tool making the actual material removal rate different for upmill and downmill cuts.

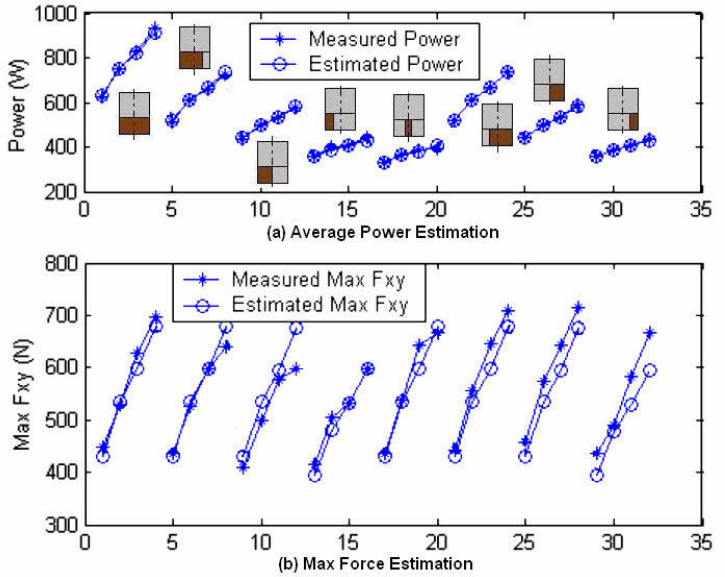

Fig. 3: Standard calibration results for flat end mill cutter.

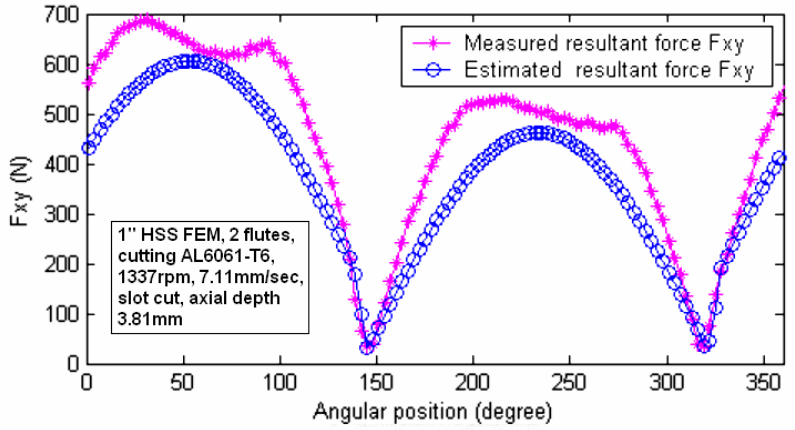

Fig. 4: Measured and estimated resultant forces for one revolution of a slot cut.

6.1.2 Ball-end Mill Test

Calibration tests for the ball portion of a ball end mill includes 28 different combinations of feedrate, axial depth and radial depth. A two flute, 12.7 mm (0.5 in) ball end cutter, rotating at 2100rpm, is used to machine 6061-T6 aluminum. Specific conditions, measured power and calculated values for $\dot{Q}$ and $\dot{A}$ are listed in Tab. 5. Best fit values for K_{TC} and K_{TE} for the ball portion of the end mill are obtained via Eqn. (4.5). Model accuracy as shown in Fig. 6. indicates good results with a standard error of 14 watts and an average percent error of around 3%. Note that a separate calibration is required, as reported in Fussell et al [9], to obtain the coefficients for the cylindrical portion of the cutter. Equation 1 can now be used to calculate the tangential force for any cutting condition.

Table 4 – 16 circular move tests; 25.4mm diameter, 2 flutes, flat end mill, HSS 30° helix angle, ω = 1337rpm, K_{TC}=693.8N/mm^2, K_{TE}=18.98N/mm, Pt=250.5W.										
No.	Cut	Circle Radius (mm)	axial depth (mm)	radial depth (mm)	Feed (mm/sec)	$\dot{Q}$ (mm^3/sec)	$\dot{A}$ (mm^2/sec)	Pm (W)	Estimated Pm (W)	Error (%)
1	Up mill	40.64	3.81	6.35	3.18	95	2539	340.5	342.7	0.7
2		40.64	3.81	6.35	4.23	126	2539	360.2	364.6	1.2
3		40.64	3.81	6.35	5.29	158	2539	383.4	386.5	0.8
4		40.64	3.81	6.35	6.35	190	2539	400.4	408.5	2.0
5	Down mill	80.01	3.81	6.35	3.18	68	2108	303.7	315.7	3.9
6		80.01	3.81	6.35	4.23	90	2108	329.6	331.3	0.5
7		80.01	3.81	6.35	5.29	113	2108	340.5	347.0	1.9
8		80.01	3.81	6.35	6.35	135	2108	356.8	362.6	1.6
9		40.64	3.81	6.35	3.18	59	1952	302.3	306.6	1.4
10		40.64	3.81	6.35	4.23	78	1952	318.7	320.2	0.5
11		40.64	3.81	6.35	5.29	98	1952	328.2	333.8	1.7
12		40.64	3.81	6.35	6.35	118	1952	346.6	347.4	0.2
13	Up mill	48.26	3.81	6.35	3.18	92	2496	339.1	339.9	0.2
14		48.26	3.81	6.35	4.23	123	2496	363.6	361.2	-0.7
15		48.26	3.81	6.35	5.29	153	2496	391.5	382.4	-2.3
16		48.26	3.81	6.35	6.35	184	2496	401.7	403.7	0.5

Tab. 4: Circular move test data.

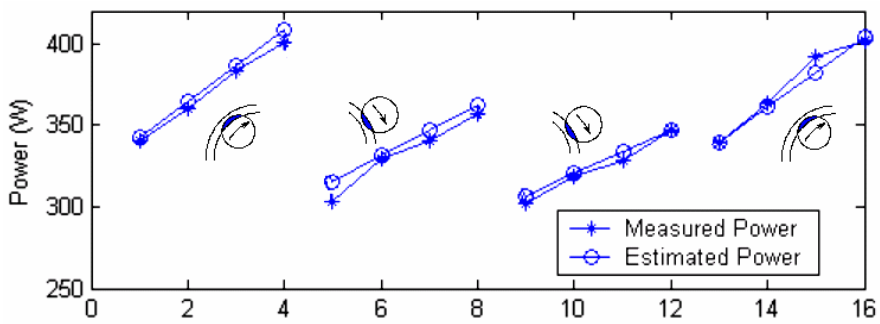

Fig. 5: Power estimation for circular moves using coefficients obtained from standard calibration test.

6.1.3 Tool Wear Effect

In our previous work, the ratio of worn tool power to sharp tool power proved to be useful to monitor tool wear [12, 22]. The model coefficient K_{TC} is related to the shearing component of the cutting force and K_{TE} is related to the rubbing or ploughing component of the cutting force. If the cutting edge does not chip or break, the power increase can mostly be attributed to the growth of the wear land (VB). Therefore, the power ratio will vary with changes in cutting geometry. The model parameters may be a better indicator for tool wear, as changes in K_{TC} will specifically show effects of cutting edge chipping or breaking and changes in K_{TE} will show effects of wear land increases.

Wear tests were performed on 1018 steel using a 12.7 mm HSS flat end mill (Weldon A16-3) at 763 rpm, with an average feed per tooth of 0.04826 mm (0.0019") and an axial depth of 3.81 mm (0.15"). A sequence of cuts containing slot, upmill (3.99 mm to 11.43 mm radial depth changing linearly with 152.4 mm tool movement), downmill (3.99 mm to 11.43 mm radial depth change), and an upmill peripheral cut at 1.27 mm (0.05") radial depth, were repeated until the tool wear land reached 0.38 mm (0.015"). Cutting power and tool wear land were measured and used to generate model constants versus cutting time.

Table 5 – 28 cutting tests; 12.7 mm diameter, 2 flutes, ball end mill, HSS 30° helix angle, ω = 2100rpm, K_{TC} = 843.2 N/mm2, K_{TE} = 15.10 N/mm, Pt = 264.2W.

No.	Cut	axial depth (mm)	radial depth (mm)	Feed (mm/sec)	$\dot{Q}$ (mm^3/sec)	$\dot{A}$ (mm^2/sec)	Pm (W)	Estimated Pm (W)
1	Slot	6.35	12.7	5.33	338	8860	668.8	666.2
2		6.35	12.7	8.00	507	8860	806.3	808.6
3		3.18	11	5.33	132	4430	434.5	425.9
4		3.18	11	8.00	198	4430	512.1	481.6
5	Up mill	6.35	9.53	5.33	272	6646	579.2	577.1
6		6.35	9.53	8.00	408	6646	696.6	691.7
7		6.35	9.53	9.61	490	6646	772.2	760.8
8		6.35	9.53	11.73	597	6646	853.1	851.7
9	Down mill	6.35	9.53	5.33	272	6646	565.7	577.1
10		6.35	9.53	8.00	408	6646	684.2	691.7
11		6.35	9.53	9.61	490	6646	763.1	760.8
12		6.35	9.53	11.73	597	6646	860.8	851.7
13	Up mill	6.35	6.35	5.33	169	4430	463.6	456.9
14		6.35	6.35	8.00	253	4430	548.7	528.1
15		6.35	6.35	9.61	304	4430	581.4	571.1
16		6.35	6.35	11.73	371	4430	645.3	627.6
17	Down mill	6.35	6.35	5.33	169	4430	436.9	456.9
18		6.35	6.35	8.00	253	4430	493.2	528.1
19		6.35	6.35	9.61	304	4430	544.4	571.1
20		6.35	6.35	11.73	371	4430	593.2	627.6
21	Up mill	5.5	3.18	5.33	66	2215	341.7	336.7
22		5.5	3.18	8.00	99	2215	369.7	364.6
23		5.5	3.18	9.61	119	2215	387.1	381.4
24		5.5	3.18	11.73	145	2215	415.9	403.4
25	Down mill	5.5	3.18	5.33	66	2215	330.8	336.7
26		5.5	3.18	8.00	99	2215	359.7	364.6
27		5.5	3.18	9.61	119	2215	381.1	381.4
28		5.5	3.18	11.73	145	2215	397.7	403.4

Tab. 5: Data of ball end mill calibration test.

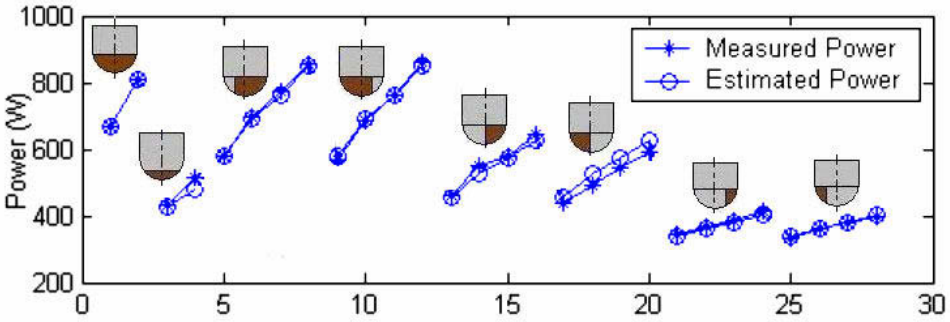

Fig. 6: Calibration results for ball end mill cutter.

Fig. 7 shows the tangential model parameters versus cutting time. Note the steady increase in K_{TE} as cutting continues and the sharp increase in K_{TC} near the end of tool life. K_{TE} can help determine the flank wearland (VB) and expected life remaining, while K_{TC} provides warning as the tooth edge starts to breakdown. Unlike commercial tool condition monitoring systems that use power threshold [2], monitoring model coefficients will simplify the process by eliminating the learning process used to establish the power threshold for every new part.

7. CONCLUSIONS

A power model based on a linear force model with edge effect is derived. The robustness of the model is verified through experiments with a wide variety of cutting conditions, results show good agreements between measured power and estimated power for both flat-end and ball-end cutting. Good agreement between estimated and measured

peak forces were obtained for flat-end cutting (max error = 16%). Force estimation for ball-end cutting was not as good (max error = 30%) and further research is required. The tangential cutting coefficients behave differently with tool wear. Experiments with a HSS flat end mill show that K_{TC} increases with edge chipping and breakage, while K_{TE} increases as the flank wearland expands.

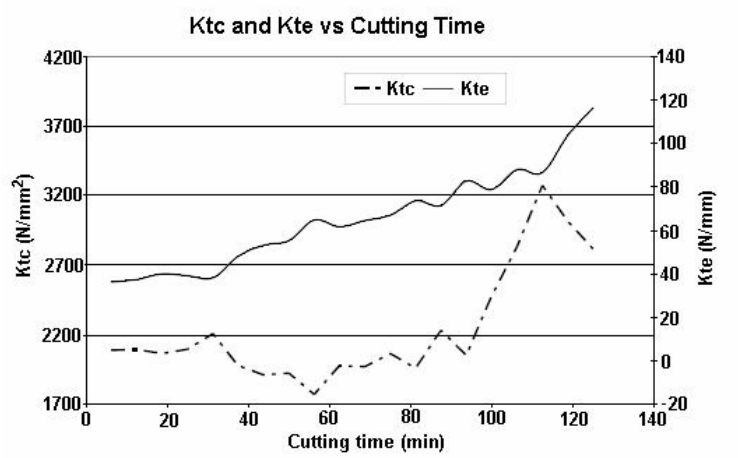

Fig. 7: Tangential cutting coefficients change with tool wear.

8. ACKNOWLEDGMENTS

The support of the National Science Foundation under grant DMI-0322869 is gratefully acknowledged. Input and guidance from Donald Esterling, President of VulcanCraft LLC of Carrboro, NC is also gratefully acknowledged.

9. REFERENCES

[1] Altintas, Y.: Manufacturing Automation: Metal Cutting Mechanics, Machine Tool Mechanics, Machine Tool Vibrations, and CNC Design, Cambridge University Press, Cambridge, United Kingdom, 2000, 33-46.

[2] Caron Engineering, Systems for tool monitoring, http://www.caron-eng.com/

[3] Azeem A.; Feng, H. Y.; Orban, P.: Processing Noisy Cutting Force Data for Reliable Calibration of a Ball-end Milling Force Model, Measurement, 38(2), 2005, 113-123.

[4] Budak, E.; Altintas, Y.; Armarego, E.: Prediction of Milling Force Coefficients From Orthogonal Cutting Data, Journal of Manufacturing Science and Engineering, Transactions of the ASME, 118(2), 1996, 216-224.

[5] Choi, B. K.; Jerard, R. B.: Sculptured Surface Machining, Kluwer Academic Publishers, 1998, 251-253, 284-286.

[6] Cuppini, D.; D'Errico, G.; Rutelli, G.: Tool Wear Monitoring Based on Cutting Power Measurement, Wear, 139, 1990, 303-311.

[7] DeVor, R. E.; Kline, W. A.; Zdeblick, W. J.: A Mechanistic Model for the Force System in End Milling with Application to Machining Airframe Structures, Proc. of the 8th North American Manufacturing Research Conference, 8, 1980, 297.

[8] Fussell, B. K.; Ersoy, C.; Jerard, R. B.: Computer Generated CNC Machining Feedrates, Proceedings of the Japan-USA Symposium on Flexible Automation, San Francisco, CA, 1992, 377–384.

[9] Fussell, B. K.; Jerard, R. B.; Hemmett, J. G.: Robust Feedrate Selection for 3-axis Machining Using Discrete Models, ASME Journal of Manufacturing Science and Engineering, 123(2), 2001, 214-224.

[10] Fussell, B. K.; Hemmett, J. G.; Jerard, R. B.: Modeling of cutting geometry and forces for 5-axis sculptured surface machining, Computer Aided Design, 35, 2003, 333-346.

[11] Jerard, R. B.; Fussell, B. K.; Ercan, M. T.; Hemmett, J. G.: Integration of Geometric and Mechanistic Models of NC Machining into an Open-Architecture Machine Tool Controller, ASME International Mechanical Engineering Congress and Exposition, Nov. 5-10, 2000.

[12] Jerard, R. B.; Fussell, B. K.; Xu, M.; Schuyler, C. K.: Smart Machine Tool Architecture, Proceedings of 2005 NSF DMII Grantees Conference, Jan. 3-6, 2005.

[13] Jerard, R. B.; Fussell, B. K.; Xu M.; Yalcin, C.: Process Simulation and Feedrate Selection for Three-axis Sculptured Surface Machining, International Journal of Manufacturing Research, 1(2), 2006, 136-156.
[14] Kline, W. A.; DeVor, R. E.: The Prediction of Cutting Forces in End Milling With Application to Cornering Cuts, Inter International Journal of Machine Tool Design & Research, 22(1), 1982, 7-22.
[15] Lee, P.; Altintas, Y.: Prediction of Ball-end Milling Forces from Orthogonal Cutting Data, International Journal of Machine Tools & Manufacture, 36(9), 1996, 1059-1072.
[16] Liu, X.-W.; Cheng, K.: Investigation of the Cutting Force Coefficients in Ball-end Milling, Laser Metrology and Machine Performance VI, 2003, 45-54.
[17] Machinability Data Center: Machining Data Handbook, 3rd ed., Institute of Advanced Manufacturing Sciences, Inc., 1980.
[18] Predator Software Inc., Predator SDK, http://www.predator-software.com/virtualcnc.htm
[19] Schmitz, T.; Ziegert, J.: Examination of Surface Location Error due to Phasing of Cutter Vibrations, Precision Engineering, 23(1), 1999, 51-62.
[20] Shao, H.; Wang, H. L.; Zhao, X. M.: A Cutting Power Model for Tool Wear Monitoring in Milling, International Journal of Machine Tools & Manufacture, 44, 2004, 1503-1509.
[21] Tlusty, J.; MacNeil, P.: Dynamics of Cutting Forces in End Milling, Annals of the CIRP, 24(1), 1975, 21-25.
[22] Xu, M.; Schuyler, C. K.; Jerard, R.B.; Fussell, B.K.: Experimental Evaluation of a Smart Machining System for Feedrate Selection and Tool Condition Monitoring, NAMRI Conference, 34, 2006.
[23] Yucesan, G.; Altintas, Y.: Mechanics of Ball End Milling Process, American Society of Mechanical Engineers, Production Engineering Division (Publication) PED, Manufacturing Science and Engineering, 64, 1993, 543-552.
[24] Zhang, Z.; Zheng, L.: A Study on Calibration of Coefficients in End Milling Forces Model", International Journal of Advanced Manufacturing Technology, 25(7-8), 2005, 652-662.